Supplementary Material for: "Near-field chiral excitation of universal spin-momentum locking transport of edge waves in microwave metamaterials"

Zhixia Xu,[a,b] Jie Chang,[b] Jinye Tong,[b] Daniel F. Sievenpiper,[c,*] Tie Jun Cui [a,*]

[a]State Key Laboratory of Millimeter Waves, Southeast University, Nanjing 210096, China
[b]School of Information Science and Technology, Dalian Maritime University, Dalian 116026, China
[c]Electrical and Computer Engineering Department, University of California San Diego, La Jolla 92093, California

*Daniel F. Sievenpiper, E-mail: dsievenpiper@eng.ucsd.edu
*Tie Jun Cui, E-mail: tjcui@seu.edu.cn

1   Feeding networks

The fabricated feeding network is shown in Fig. S1, consisting of Wilkinson dividers and phase shifters. Port5 is the input port, and Ports1-4 are output ports with the same magnitude and phase difference. Three ultra-broadband Wilkinson dividers need seven isolation resistors (R_{1-7} = 240, 130, 220, 330, 430, 620, 430 Ω). The overall width W_1 is 60 mm, and the length L_6 is 159.2 mm. W_8 and L_1 are 1.1 mm and 41.356 mm. The phase-shifters consist of a multimode resonator and two branches connected with ground by via, realizing a signal difference of 90 or 180 degrees. L_2, L_3, L_4, and L_5 are 40.1, 2, 33.9, and 0.6 mm, W_2, W_3, W_4, W_5, W_6, and W_7 are 5.2, 0.5, 0.1, 4.3, 0.8, and 0.4 mm. The substrate used is Rogers 4350B with permittivity of 3.48 and thickness of 0.508 mm.
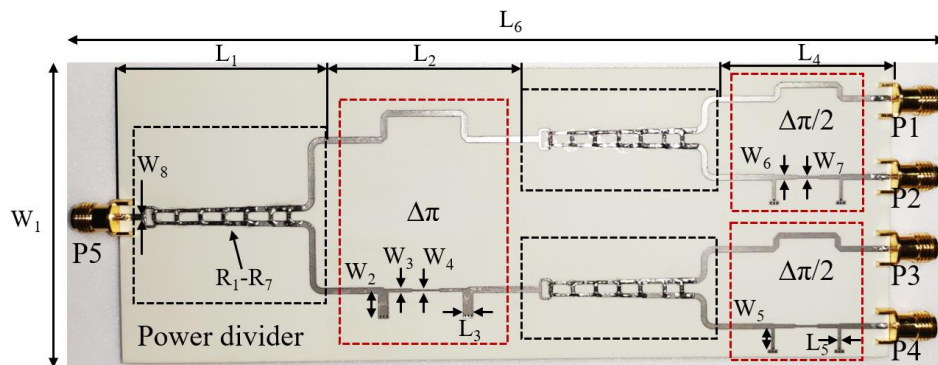

Fig. S1 The fabricated phase-shifting power divider.

2   Parameters of metamaterials

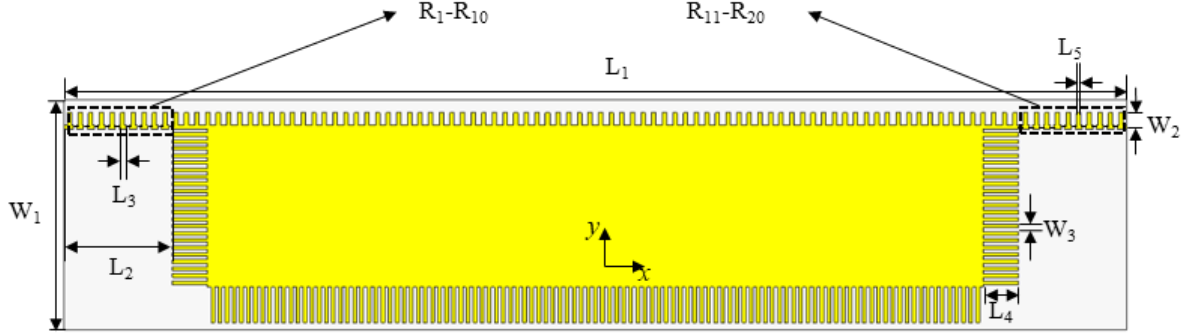We give detailed parameters of designed metamaterials in Figs. S2-4.

Fig. S2 Detailed structure of the Spoof SPPs. The geometric parameters are listed below: the thickness of copper is 0.035mm, the length L_1 is 300mm, the length L_2 is 29.5mm, the length L_3 is 2mm, the length L_4 is 10mm, the length L_5 is 1.2mm, the widths W_1, W_2, and W_3 are 65mm, 4.7mm, and 1mm. The resistance R_1, R_2, R_{19}, and R_{20} are 10Ω, the resistance R_3, R_4, R_{17}, and R_{18} are 15Ω, the resistance R_5, R_6, R_{15}, and R_{16} are 20Ω, the resistance R_7, R_8, R_{13}, and R_{14} are 25Ω, the resistance R_9, R_{10}, R_{11}, and R_{12} are 30Ω. The substrate used is polyimide with a relative permittivity of 4.1 and thickness of 0.2mm.
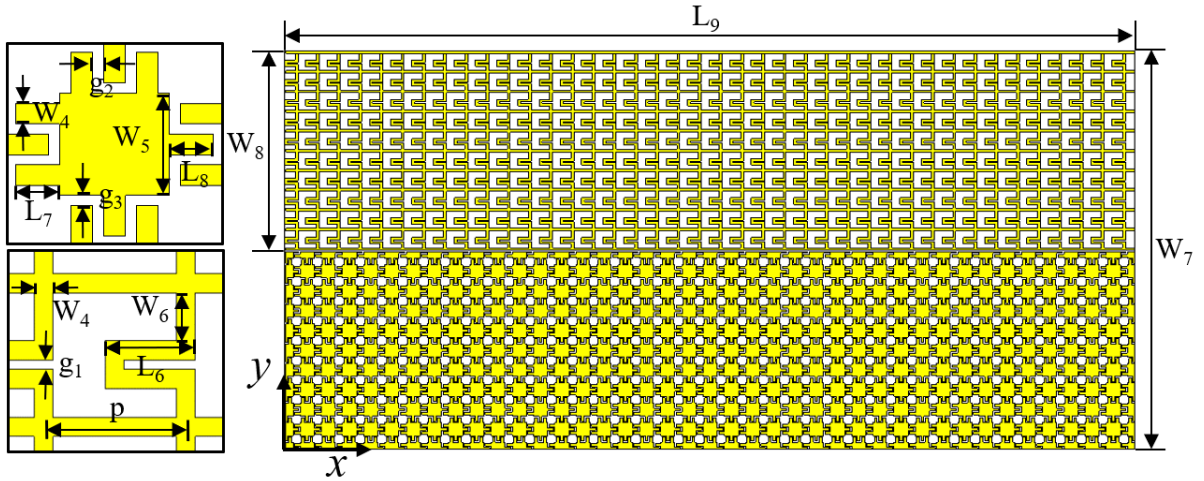

Fig. S3 Detailed structure of the LWs model. The geometric parameters are listed below: the thickness of copper is 0.035mm, the periodic length p is 3mm, the length L_6, L_7, L_8 and L_9 is 1.9mm, 0.8mm, 0.8mm, and 120mm, the width is, the widths W_4, W_5, W_6, W_7, and W_8 are 0.4mm, 2mm, 1mm, 60.2mm and 30.1mm, the gap g_1, g_2, and g_3 are 0.2mm. The substrate used in this work is polyimide with a relative permittivity of 4.1 and thickness of 0.2mm.
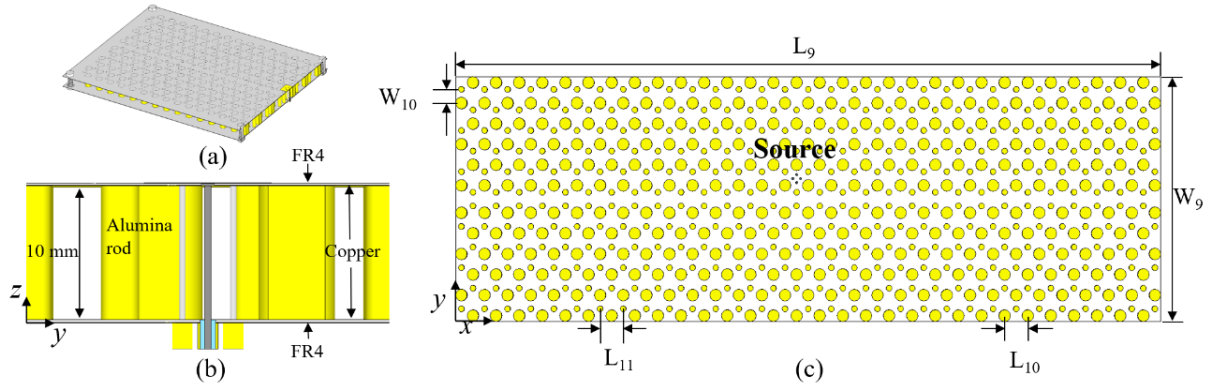
Fig. S4 Detailed structure of valley PTIs model. (a)The side view with cross-section. (b) The view on the *y-z* plane. The bottom is copper, which is connected to the outer conductor of the coaxial line. Above the copper is FR4. Above the alumina rod is copper, which is connected to the inner conductor of the coaxial line. Above the copper is FR4. (c) The structure consists of 300 ceramics cylinders with a diameter of 3mm and 300 cylinders with a diameter of 6mm. The alumina rods are inserted between the two plates. The lengths L_9, L_{10}, and L_{11} are 366mm, 12mm, and 12mm. The width W_9 and W_{10} are $(68\sqrt{3}+6)$mm and $4\sqrt{3}$mm. The relative permittivity and thickness of the FR4 are 4.3 and 0.2mm. The thickness of copper is 0.035mm. The height of the alumina rod is 10mm.

3   Simulations

3.1 Spoof SPPs

The eigenmode solver of the CST Studio Suite is used to obtain the dispersion curves of spoof SPPs. Unit cells are shown in Fig. S5. Boundaries along *y*-direction and *z*-direction are set as electric boundary condition. Electric boundaries are more than λ/4 away from the structure to preclude unwanted modes caused by boundaries. Boundaries along *x*-direction are set as periodic boundary condition.
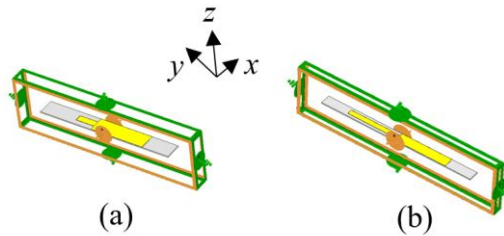

Fig. S5 Unit cell simulation setup of (a) SSPPs-1 and (b) SSPPs-2.

The entire structure is excited by circular-polarized (CP) dipoles, as shown in Fig. S6(a). The CP source is located at the center of the structure and 7.5 mm away from the edge. Two dipole antennas with a phase difference of 90 degrees are used to generate the CP waves. The time domain solver of CST Studio Suite is used for full model simulations. The boundary condition is set as open (add space) in all directions. Electric field monitors are set to observe electric field distribution. The conformal model is shown in Fig. S6(b).
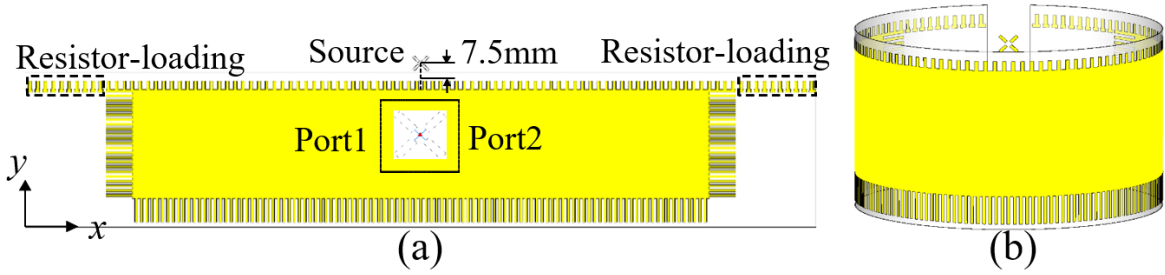

Fig. S6 (a) The planar SSPPs model. (b) The conformal SSPPs model.

3.2 LWs

The eigenmode solver of CST Studio Suite is used to obtain dispersion curves of the inductive and capacitive unit cells. The detailed structure and boundary conditions are shown in Fig. S7 (a) and (b). Boundaries along *x*-direction and y-direction are set as periodic boundary condition. Boundaries along *z*-direction are set as electric boundary condition. We further calculate the equivalent surface impedance according to Eq. S1 and Eq. S2.

$$Z_{\text{TM}} = \eta_0 \sqrt{1 - \frac{k_t^2}{k_0^2}} \tag{S1}$$

$$Z_{\text{TE}} = \eta_0 \Big/ \sqrt{1 - \frac{k_t^2}{k_0^2}} \tag{S2}$$

where k_t is the wavevector along the surface, k_0 is the wavevector in vacuum, and η_0 is the surface impedance in vacuum. The full-model is shown in Fig. S8. CP source is placed at the center of the structure, 4 mm under the Z_{TE} surface, and 4.3mm away from the edge.
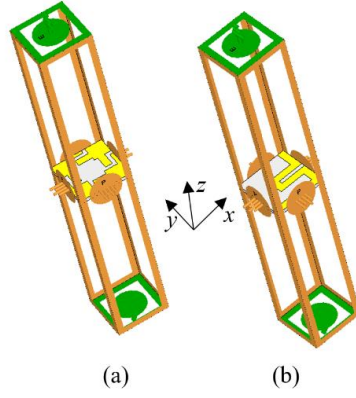
4

(a)   (b)

Fig. S7 (a) Detailed structure of the proposed capacitive unit cell. (b) Detailed structure of the proposed inductive unit cell.
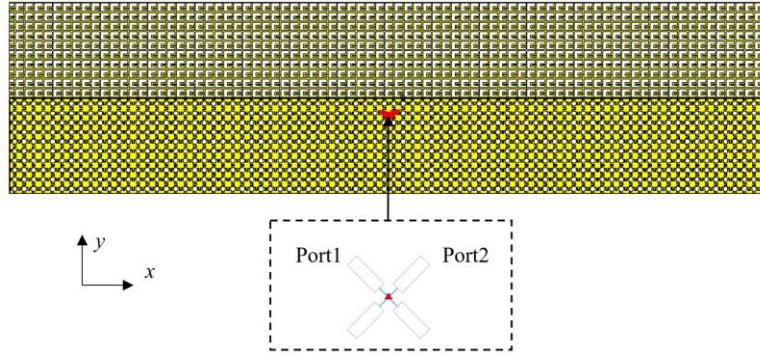

Fig. S8 The detailed structure of the Z_{TE} and Z_{TM} metasurface with CP dipoles.

3.3 Valley PTIs

2D eigen mode simulation is conducted in Comsol Multiphysics. The detailed geometric parameters and boundary conditions are shown in Fig. S9. The permittivity of dielectric rods in simulation is set as 7.8 to match the measured results. The value is a bit lower than real alumina because there exists gap between dielectric rods and conductor-plate in the fabricated sample, which causes the effective permittivity decreases. In order to calculate valley freedom of topological invariant, we discretize Brillouin Zone, as shown in Fig. S10 and then use four-point formula to calculate Berry curvature as below.

$$\phi = -\text{Im} \log[\langle u_{k1}(\mathbf{r})|u_{k2}(\mathbf{r})\rangle\langle u_{k2}(\mathbf{r})|u_{k3}(\mathbf{r})\rangle\langle u_{k3}(\mathbf{r})|u_{k4}(\mathbf{r})\rangle\langle u_{k4}(\mathbf{r})|u_{k1}(\mathbf{r})\rangle] \quad \text{(S3)}$$

5

where $E_{Z,k}(\mathbf{r}) = e^{i\mathbf{k}\cdot\mathbf{r}}u_{\mathbf{k}}(\mathbf{r})$. Based on periodic boundary conditions, the solution of eigen-problems is be expressed as Bloch states with wave vector $\mathbf{k}$. Comsol-Matlab-livelink function is used to extract simulated field distributions and input them into Matlab for further calculation. 2D full models with OAM point sources are established in COMSOL, as shown in Fig. S11. Current-source array at the center of one unit cell is used to generate OAM waves by setting the handedness of phase distributions. The normalized amplitude of electric field at the two different terminals are plotted. In order to confirm the correctness of 2D model approximation, we establish a 3D model in CST Studio Suite as a comparison, as shown in Fig. S12. Results match well with Fig. S11, verifying the correctness of 2D model approximation. Movies of simulation of spoof SPPs and LWs are extracted from CST Studio Suite, and movies of simulation of valley PTIs are extracted from COMSOL.
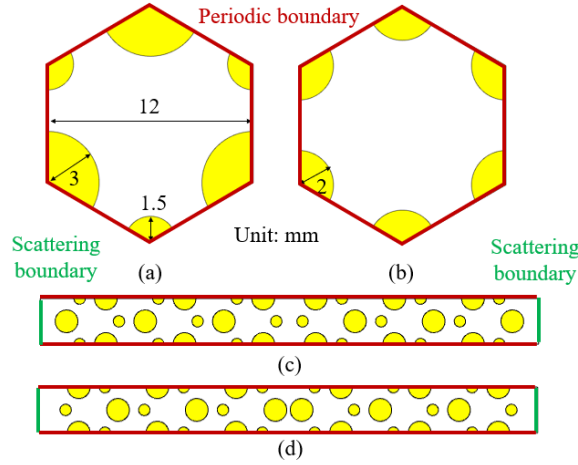

Fig. S9 Unit cell: (a) valley PTIs, (b) trivial photonic crystals. Super lattice: (c) Type-1 edge (fabricated sample). (d) Type-2 edge.
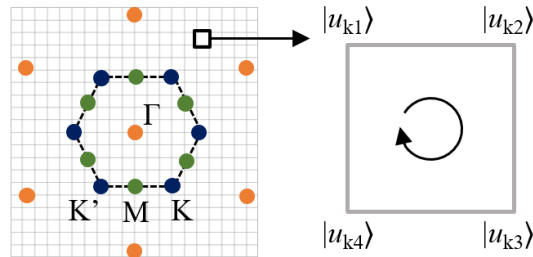

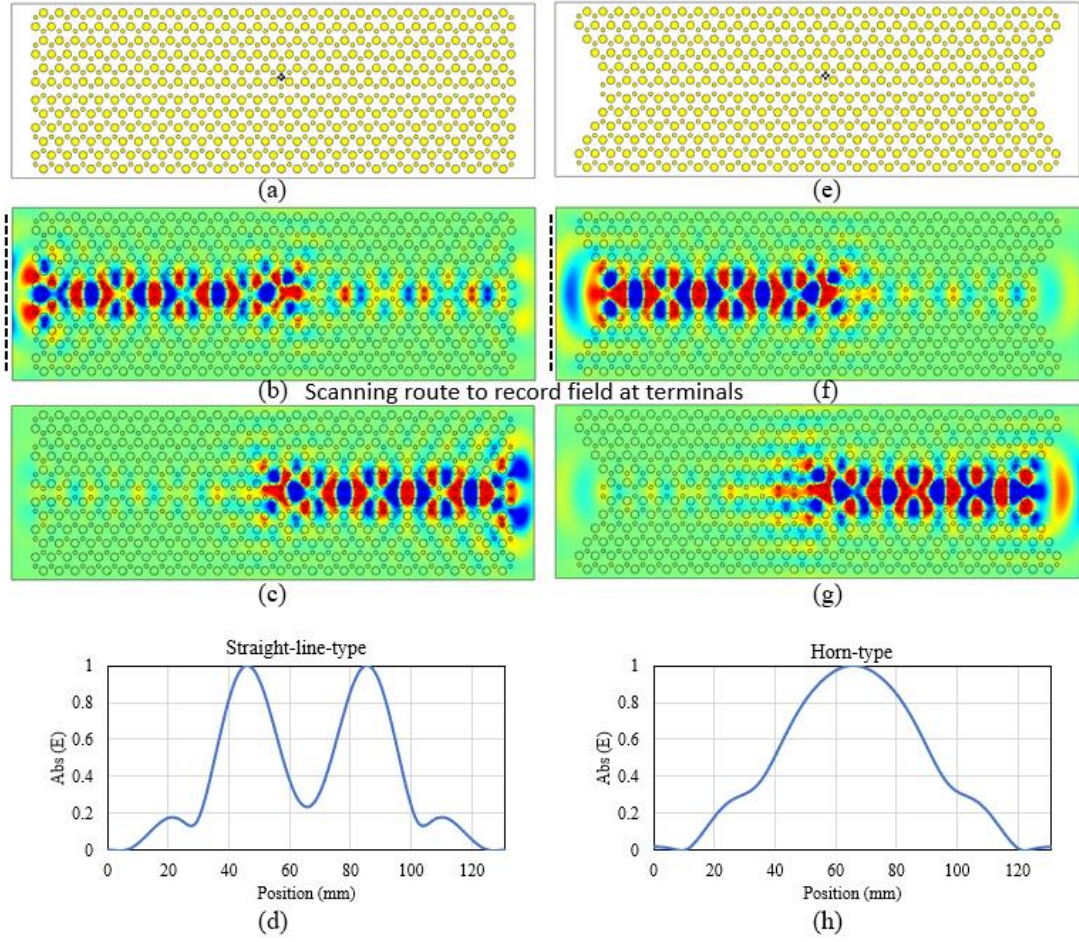**Fig. S10** Discretization of the 1st BZ and the four-point formula procedure.

6

Fig. S11 Straight-line-type terminal: (a) model, (b) left transports, (c) right transports, (d) normalized electric field. Horn-type terminal: (e) model, (f) left transports, (g) right transports, (h) normalized electric field.
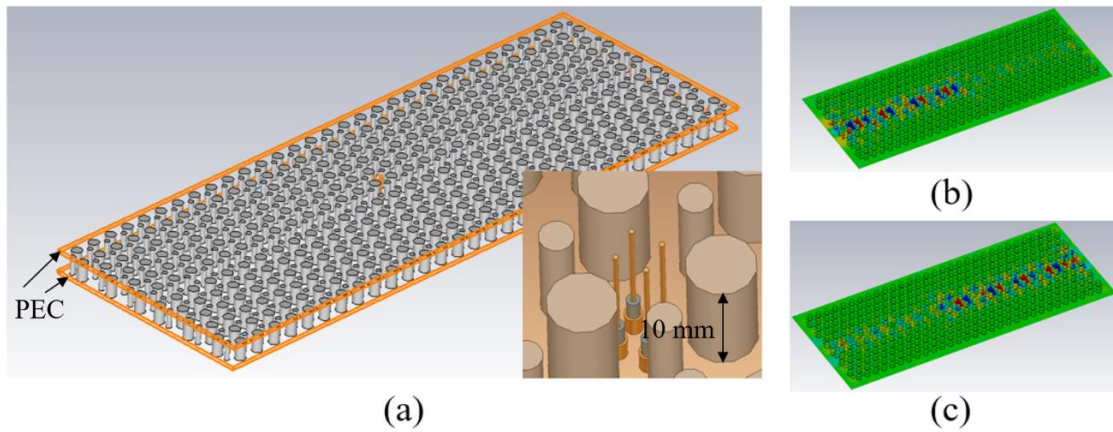

Fig. S12 (a) 3D full model in CST Studio Suite, (b) left transports, (c) right transports. The height of dielectric rod is set as 10 mm, and the permittivity of dielectric rod is set as 7.8, and the top and bottom plate of valley PTIs waveguide is set as PEC.

Two sets of OAM sources are studied to investigate the influence of OAM charge $|\ell|$ and phase stepping $\Delta\varphi$ on unidirectional coupling, as shown in Fig. S13. The integral of the Poynting flow is calculated in COMSOL to obtain the input and output energy (P_{source}, P_{left}, P_{right}). We define P_{left}/P_{source} and P_{right}/P_{source} as transmission. As examples, two OAM sources ($\ell=1$, $\Delta\varphi=\pi/2$) and ($\ell=2$, $\Delta\varphi=\pi/2$) are compared in Fig. S13(c). Moreover, valley unit cell carries only fundamental OAM ($\ell = \pm1$) because we can calculate phase relationships between different lattice sites, as shown in Fig. S13(d). Phase shift $\Delta\varphi_1$ and $\Delta\varphi_2$ are determined by $\boldsymbol{k}\cdot\boldsymbol{r}_1$ and $\boldsymbol{k}\cdot\boldsymbol{r}_2$. The $\Delta\varphi_1$ and $\Delta\varphi_2$ are $2\pi/3$ and $4\pi/3$ at K point, and $4\pi/3$ and $2\pi/3$ at K' point, which is consistent with ($\ell = \pm1$).
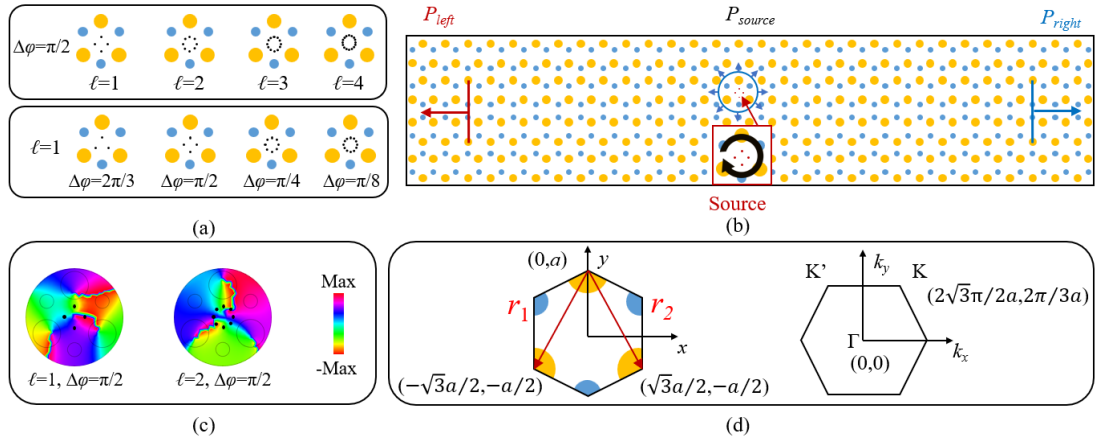

Fig. S13 (a) Various OAM sources. (b) Full model. (c) OAM phase distributions. (d) Unit cell and Brillouin zone which decides that the intrinsic OAM ($\ell = \pm1$).

4   Experiments

As is shown in Fig. S14, the experimental platform is composed of one vector network analyzer (VNA), one PC, one microcontroller, two Micro-step Drivers, one power supply, and one rail measurement unit. PC controls both microcontroller and VNA. PC is connected to VNA by TCP/IP interface. MATLAB is used to set up the parameters of the VNA, read S-parameters from VNA, and control the direction and distance of the rail movement.
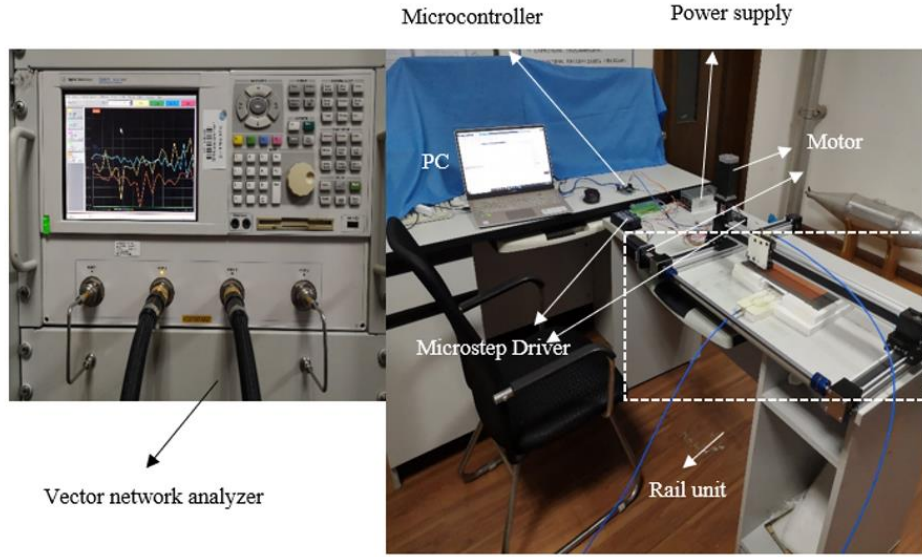
Fig. S14 Near-field testing platform.

5　Discussion of measured LWs

Measurements of unidirectional LWs show some discrepancies with simulations. This experiment is the most challenging, and it is the first experiments to observe the unidirectional LWs. The difficulty is mainly caused by the unwanted excitation of TE/TM surface modes in metasurfaces. We illustrate the challenge in Fig. S15. It is obvious that the leakage towards bulk is forbidden in both spoof SPPs and PTIs. However, the overlapping of dispersion of LWs, TE-/TM-polarized surfaces waves caused unwanted transmission on the metasurface. The probe used in experiments is not an ideal model in simulations; therefore, these surface waves can be excited and hard to suppress.
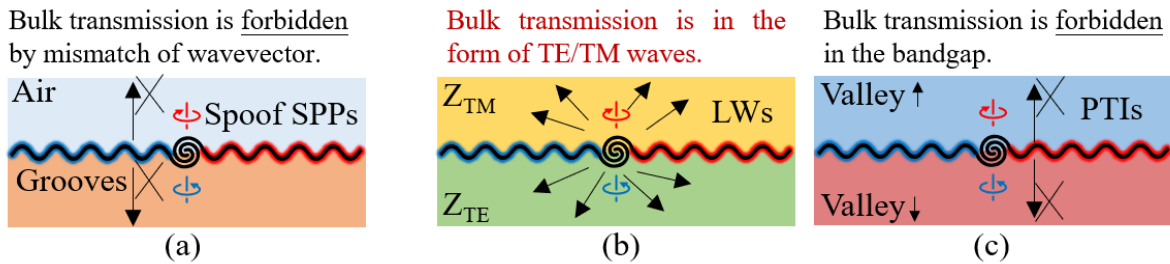

Fig. S15. Bulk transmission is (a) forbidden in Spoof SPPs, (b) supported in LWs, and (c) forbidden in PTIs.